24. Herrlinger, U.; Schaefer, N; Steinbach, J.P.; Weyerbrock, A.; Hau, P.; Goldbrunner, R.; Friedrich, F.; Stockhammer, F.; Ringel, F.; *et al.* Bevacizumab, irinotecan, and radiotherapy *versus* standard temozolomide and radiotherapy in newly diagnosed, MGMT-non-methylated glioblastoma patients: First results from the randomized multicenter GLARIUS trial. American Society for Clinical Oncology (ASCO), Chicago, USA. 1 June 2013, Abstract #LBA2000.
25. Reardon, D.A.; Desjardins, A.; Peters, K.; Gururangan, S.; Sampson, J.; Rich, J.N.; McLendon, R.; Herndon, J.E., II; Marcello, J.; Threatt, S.; *et al.* Phase II study of metronomic chemotherapy with bevacizumab for recurrent glioblastoma after progression on bevacizumab therapy. *J. Neurooncol.* **2011**, *103*, 371–379.
26. Reardon, D.A.; Desjardins, A.; Peters, K.B.; Vredenburgh, J.J.; Gururangan, S.; Sampson, J.H;. McLendon, R.E.; Herndon, J.E., 2nd; Coan, A.; Threatt, S.; *et al.* Phase 2 study of carboplatin, irinotecan, and bevacizumab for recurrent glioblastoma after progression on bevacizumab therapy. *Cancer* **2011**, *117*, 5351–5358.
27. Quant, E.C.; Norden, A.D.; Drappatz, J.; Muzikansky, A.; Doherty, L.; Lafrankie, D.; Ciampa, A.; Kesari, S.; Wen, P.Y. Role of a second chemotherapy in recurrent malignant glioma patients who progress on bevacizumab. *Neuro-oncology* **2009**, *11*, 550–555.
28. Zuniga, R.M.; Torcuator, R.; Jain, R.; Anderson, J.; Doyle, T.; Schultz, L.; Mikkelsen, T. Rebound tumour progression after the cessation of bevacizumab therapy in patients with recurrent high-grade glioma. *J. Neurooncol.* **2010**, *99*, 237–242.
29. Chamberlain, M.C. Bevacizumab for the treatment of recurrent glioblastoma. *Clin. Med. Insights Oncol.* **2011**, *5*, 117–129.
30. Kesselheim, J.C.; Norden, A.D.; Wen, P.Y.; Joffe, S. Discontinuing bevacizumab in patients with glioblastoma: An ethical analysis. *Oncologist* **2011**, *16*, 1435–1439.
31. Reardon, D.A.; Wen, P.Y.; Desjardins, A.; Batrchelor, T.T.; Vredenburgh, J.J. Glioblastoma multiforme: An emerging paradigm of anti-VEGF therapy. *Expert Opin. Boil. Ther.* **2008**, *8*, 541–553.
32. Bennouna, J.; Sastre, J.; Arnold, D.; Oesterlund, P.; Greil, R.; van Cutsem, E.; von Moos, R.; Vieitez, J.M.; Bouche, O.; Borg, C.; *et al.* Continuation of bevacizumab after first progression in metastatic colorectal cancer (ML18147): A randomised phase 3 trial. *Lancet Oncol.* **2013**, *14*, 29–37.
33. Reardon, D.A.; Herndon, J.E., 2nd; Peters, K.B.; Desjardins, A.; Coan, A.; Lou, E.; Sumrall, A.L.; Turner, S.; Lipp, E.S.; Sathornsumetee, S.; *et al.* Bevacizumab continuation beyond initial bevacizumab progression among recurrent glioblastoma patients. *Br. J. Cancer* **2012**, *107*, 1481–1487.
34. Omuro, A.; Chan, T.A.; Abrey, L.E.; Khasraw, M.; Reiner, A.S.; Kaley, T.J.; Deangelis, L.M.; Lassman, A.B.; Nolan, C.P.; Garvilovic, I.T.; *et al.* Phase II trial of continuous low-dose temozolomide for patients with recurrent malignant glioma. *Neuro-oncology* **2013**, *15*, 242–250.
35. Piccioni, D.E., Selfridge, J., Mody, R., Quan, J., Zurayk, M., Li, S., Chen, W., Chou, A., Liau, L., Green, R., *et al.*, Eds.; Deferred use of bevacizumab for recurrent glioblastoma is not associated with diminished efficacy. In Proceedings of the 17th Annual Scientific Meeting and Education Day of the Society for Neuro-Oncology (SNO), Washington, DC, USA, 16 November 2012; Oxford University Press: Oxford, UK, 2012; Abstract #NO-97.

36. Wen, P.Y.; Macdonald, D.R.; Reardon, D.A.; Cloughesy, T.F.; Sorensen, A.G.; Galanis, E.; Degroot, J.; Wick, W.; Gilbert, M.R.; Lassman, A.B.; *et al.* Updated response assessment criteria for high-grade gliomas: Response assessment in neuro-oncology working group. *J. Clin. Oncol.* **2010**, *28*, 1963–1972.
37. Holash, J.; Maisonpierre, P.C.; Compton, D.; Boland, P.; Alexander, C.R.; Zagzag, D.; Yancopoulos, G.D.; Wiegand, S.J. Vessel cooption, regression, and growth in tumors mediated by angiopoietins and VEGF. *Science* **1999**, *284*, 1994–1998.
38. Iwamoto, F.M.; Abrey, L.E.; Beal, K.; Gutin, P.H.; ROsenblum, M.K.; Reuter, V.E.; DeAngelis, L.M.; Lassman, A.B. Patterns of relapse and prognosis after bevacizumab failure in recurrent glioblastoma. *Neurology* **2009**, *73*, 1200–1206.
39. Norden, A.D.; Young, G.S.; Setayesh, K.; Muzikansky, A.; Klufas, R.; Ross, G.L.; Clampa, A.S.; Ebbeling, L.G.; Levy, B.; Drappatz, J.; *et al.* Bevacizumab for recurrent malignant gliomas: Efficacy, toxicity, and patterns of recurrence. *Neurology* **2008**, *70*, 779–787.
40. Pope, W.B.; Xia, Q.; Das, A.; Hambleton, J.; Kim, H.; Brwon, M.; Goldin, J.; Coughesy, T.F. Patterns of progression in patients with glioblastoma at first or second relapse treated with bevacizumab alone or in combination with irinotecan in the BRAIN study. *Neuro-oncology* **2009**, *11*, 626 (Abstract # 270 from the 2009 Joint Meeting of SNO and AANS/CNS Section on Tumors).
41. Chamberlain, M.C. Radiographic patterns of relapse in glioblastoma. *J. Neurooncol.* **2011**, *101*, 319–323.
42. Wick, W.; Cloughesy, T.F.; Nishikawa, R.; Mason, W.; Saran, F.; Henriksson, R.; Hilton, M.; Kerloeguen, Y.; Chino, O.L. Tumor response based on adapted Macdonald criteria and assessment of pseudoprogression (PsPD) in the phase III AVAglio trial of bevacizumab (Bv) plus temozolomide (T) plus radiotherapy (RT) in newly diagnosed glioblastoma (GBM). American Society for Clinical Oncology (ASCO), Chicago, IL, USA, 1 June 2013, Abstract #2002.
43. Wong, E.T.; Gautam, S.; Malchow, C.; Lun, M.; Pan, E.; Brem, S. Bevacizumab for recurrent glioblastoma multiforme: A meta-analysis. *J. Natl. Compr. Canc. Netw.* **2011**, *9*, 403–407.
44. Bocci, G.; Loupakis, F. The possible role of chemotherapy in antiangiogenic drug resistance. *Med. Hypotheses* **2012**, *78*, 646–648.
45. Grothey, A.; Sugrue, M.M.; Purdie, D.M.; Dong, W.; Sargent, D.; Hendrick, E.; Kozloff, M. Bevacizumab beyond first progression is associated with prolonged overall survival in metastatic colorectal cancer: Results from a large observational cohort study (BRiTE). *J. Clin. Oncol.* **2008**, *26*, 5326–5334.
46. Ebos, J.M.; Lee, C.R.; Cruz-Munoz, W.; Bjamason, G.A.; Christensen, J.G.; Kerbel, R.S. Accelerated metastasis after short-term treatment with a potent inhibitor of tumor angiogenesis. *Cancer Cell* **2009**, *15*, 232–239.
47. Paez-Ribes, M.; Allen, E.; Hudock, J.; Takeda, T.; Okuyama, H.; Vinals, F.; Inoue, M.; Bergers, G.; Hanahan, D.; Casanovas, O. Antiangiogenic therapy elicits malignant progression of tumors to increased local invasion and distant metastasis. *Cancer Cell* **2009**, *15*, 220–231.
48. Gherardi, E.; Birchmeier, W.; Birchmeier, C.; Vande Woude, G. Targeting MET in cancer: Rationale and progress. *Nat. Rev. Cancer* **2012**, *12*, 89–103.

49. Pennacchietti, S.; Michieli, P.; Galluzzo, M.; Mazzone, M.; Giordano, S.; Comoglio, P.M. Hypoxia promotes invasive growth by transcriptional activation of the met protooncogene. *Cancer Cell* **2003**, *3*, 347–361.
50. Thiery, J.P.; Acloque, H.; Huang, R.Y.; Nieto, M.A. Epithelial-mesenchymal transitions in development and disease. *Cell* **2009**, *139*, 871–890.
51. Yilmaz, M.; Christofori, G. Mechanisms of motility in metastasizing cells. *Mol. Cancer Res.* **2010**, *8*, 629–642.
52. Lu, K.V.; Chang, J.P.; Parachoniak, C.A.; Pandika, M.M.; Aghi, M.K.; Meyronet, D.; Isachenko, N.; Fouse, S.D.; Phillips, J.J.; Cheresh, D.A.; *et al.* VEGF inhibits tumor cell invasion and mesenchymal transition through a MET/VEGFR2 complex. *Cancer Cell* **2012**, *22*, 21–35.
53. Cooke, V.G.; LeBleu, V.S.; Keskin, D.; Khan, Z.; O'Conneill, J.T.; Teng, Y.; Duncan, M.B.; Xie, L.; Maeda, G.; Vong, S.; *et al.* Pericyte depletion results in hypoxia-associated epithelial-to-mesenchymal transition and metastasis mediated by met signaling pathway. *Cancer Cell* **2012**, *21*, 66–81.
54. Narayana, A.; Kelly, P.; Golfinos, J.; Parker, E.; Johnson, G.; Knopp, E.; Zagzag, D.; Fischer, I.; Raza, S.; Medabalmi, P.; *et al.* Antiangiogenic therapy using bevacizumab in recurrent high-grade glioma: Impact on local control and patient survival. *J. Neurosurg.* **2009**, *110*, 173–180.
55. You, W.K.; Sennino, B.; Williamson, C.W.; Falcon, B.; Hashizume, H.; Yao, L.C.; Aflab, D.T.; McDonald, D.M. VEGF and c-Met blockade amplify angiogenesis inhibition in pancreatic islet cancer. *Cancer Res.* **2011**, *71*, 4758–4768.
56. Sennino, B.; Ishiguro-Oonuma, T.; Wei, Y.; Naylor, R.M.; Williamson, C.W.; Bhagwandin, V.; Tabruyn, S.P.; You, W.K.; Chapman, H.A.; Christensen, J.G.; *et al.* Suppression of tumor invasion and metastasis by concurrent inhibition of c-Met and VEGF signaling in pancreatic neuroendocrine tumors. *Cancer Discov.* **2012**, *2*, 270–287.
57. Yakes, F.M.; Chen, J.; Tan, J.; Yamaguchi, K.; Shi, Y.; Yu, P.; Qian, F.; Chu, F.; Bentzien, F.; Cancilla, B.; *et al.* Cabozantinib (XL184), a novel MET and VEGFR2 inhibitor, simultaneously suppresses metastasis, angiogenesis, and tumor growth. *Mol. Cancer Ther.* **2011**, *10*, 2298–2308.
58. Kurzrock, R.; Sherman, S.I.; Ball, D.W.; Forastiere, A.A.; Cohen, R.B.; Mehra, R.; Phister, D.G.; Cohen, E.E.; Janisch, L.; Nauling, F.; *et al.* Activity of XL184 (Cabozantinib), an oral tyrosine kinase inhibitor, in patients with medullary thyroid cancer. *J. Clin. Oncol.* **2011**, *29*, 2660–2666.
59. Aftab, D.T.; McDonald, D.M. MET and VEGF: Synergistic targets in castration-resistant prostate cancer. *Clin. Transl. Oncol.* **2011**, *13*, 703–709.

Int J Clin Oncol
DOI 10.1007/s10147-013-0517-x

ORIGINAL ARTICLE

Predictive significance of mean apparent diffusion coefficient value for responsiveness of temozolomide-refractory malignant glioma to bevacizumab: preliminary report

Motoo Nagane · Keiichi Kobayashi · Masaki Tanaka · Kazuhiro Tsuchiya · Yukiko Shishido-Hara · Saki Shimizu · Yoshiaki Shiokawa

Received: 24 September 2012 / Accepted: 25 December 2012

Abstract
Background Recurrent glioblastoma after initial radiotherapy plus concomitant and adjuvant temozolomide is problematic. Here, patients with temozolomide-refractory high-grade gliomas were treated with bevacizumab (BV) and evaluated using apparent diffusion coefficient (ADC) for response.
Methods Nine post-temozolomide recurrent or progressive high-grade glioma patients (seven with glioblastoma and two with anaplastic astrocytoma) were treated with BV monotherapy. Average age was 57 years (range, 22–78), median Karnofsky Performance Scale (KPS) was 70 (30–80) and median BV line number was 2 (2–5). Two had additional stereotactic radiotherapy within 6 months prior to BV. Magnetic resonance (MR) imaging after BV therapy was performed within 2 weeks with calculation of mean ADC (mADC) values of enhancing tumor contours.
Results Post-BV treatment MR imaging showed decreased tumor volumes in eight of nine cases (88.9 %). Partial response was obtained in four cases (44.4 %), four cases had stable disease, and one had progressive disease. Of 15 evaluable enhancing lesions, 11 shrank and four did not. Pretreatment mADC values were above 1100 (10^{-6} mm^2/s) in all responding tumors, while all non-responding lesions scored below 1100 ($p = 0.001$). mADC decreased after the first BV treatment in all lesions except one. KPS improved in four cases (44.4 %). Median progression-free survival and overall survival for those having all lesions with high mADC (>1100) were significantly longer than those with a low mADC (<1100) lesion ($p = 0.018$ and 0.046, respectively).
Conclusions Bevacizumab monotherapy is effective in patients with temozolomide-refractory recurrent gliomas and tumor mean ADC value can be a useful marker for prediction of BV response and survival.

Keywords Glioblastoma · Bevacizumab · Apparent diffusion coefficient · Prediction of response and survival · Recurrent high-grade glioma

Introduction

Standard care for glioblastoma (GBM) is radiation therapy (RT) plus concomitant and adjuvant temozolomide (TMZ) [1]. The median overall survival (OS) of patients with GBM remains at 15 months from initial diagnosis [1], and there are no standard therapies established for recurrent GBMs.

These data were previously presented at the 2011 Annual Meeting of American Society of Clinical Oncology (ASCO), Chicago, USA, 4 June 2011, and the 16th Annual Meeting of the Society for Neuro-Oncology (SNO), Anaheim, USA, 18–21 November 2011.

M. Nagane (✉) · K. Kobayashi · M. Tanaka · S. Shimizu · Y. Shiokawa
Department of Neurosurgery, Kyorin University Faculty of Medicine, 6-20-2 Shinkawa, Mitaka, Tokyo 181-8611, Japan
e-mail: mnagane.g@gmail.com

K. Tsuchiya
Department of Radiology, Kyorin University Faculty of Medicine, 6-20-2 Shinkawa, Mitaka, Tokyo 181-8611, Japan

Y. Shishido-Hara
Department of Pathology, Kyorin University Faculty of Medicine, 6-20-2 Shinkawa, Mitaka, Tokyo 181-8611, Japan

Published online: 26 January 2013

Glioblastoma is highly vascularized and vascular endothelial growth factor (VEGF) has been identified as the major promoting factor for glioma angiogenesis [2]. VEGF expression correlates with aggressiveness and histopathological grade of glioma [3]. VEGF induces an increase in vascular permeability and disruption of the blood–brain barrier (BBB) in tumors. High-grade gliomas with abundant VEGF expression exhibit an increase in interstitial fluids, causing peri- and intra-tumoral edema [4], and further neurological deterioration. It would, therefore, be reasonable to target VEGF as a potential therapeutic strategy against intractable GBM [5].

Bevacizumab (BV) is a humanized monoclonal antibody that binds to and inhibits the activity of VEGF. The efficacy of BV for recurrent GBM was demonstrated in initial phase II clinical trials in combination with irinotecan [6]. BV monotherapy for patients with TMZ-pretreated, recurrent GBM achieved progression-free survival (PFS) at 6 months (PFS-6 m) of 43 % and median OS of 9.3 months [7]. This and another similar phase II study [8] led to accelerated approval for use of BV as a single-agent in adults with recurrent GBM in the United States. However, a subset of GBM lesions do not respond to BV, and this necessitates a way to differentiate tumors that will respond from those that will not, given the adverse effects of BV such as intracerebral hemorrhage and deep venous thrombosis, and also the high cost of the agent.

Bevacizumab decreases interstitial fluid load in the brain and tumor tissue by normalizing the BBB, leading to rapid tumor shrinkage with reduction of perifocal edema [5, 7]. An imaging technique that specifically detects such pathological conditions would be useful for prediction of BV response. One physiological imaging biomarker that might be associated with degradation of cellular integrity, such as necrosis, is apparent diffusion coefficient (ADC) obtained on diffusion-weighted magnetic resonance (MR) imaging. The ADC value represents movement of water molecules and tends to be low in tissues with high cellular density (packed tumor) where extracellular space is restricted [9]. Conversely, tissue edema and necrotic components induced by tumor burden and cytotoxic therapies may well increase the ADC value [10, 11]. The ADC value has been shown to correlate with response to radiation therapy (RT) and prognosis in patients with glioma [12, 13], to predict progression-free survival (PFS) after BV treatment in patients with recurrent GBM, and the minimum ADC values were reportedly prognostic of outcomes in glioma [12, 14]. This prompted us to investigate whether the ADC value in recurrent high-grade glioma may predict rapid shrinking response or survival after BV monotherapy, thereby facilitating selection of patients who are likely responders.

Patients and methods

Patient eligibility

Patients (≥20 years old) had histologically proven high-grade glioma (HGG) for which they had received RT and TMZ. All had experienced tumor progression determined by the Macdonald criteria [15], had measurable enhancing disease(s) on MR imaging, and had recovered from their prior treatment. The minimum 4 weeks from surgical therapy and 8 weeks after RT must have elapsed before the start of BV treatment. The patients had to have adequate organ functions and were excluded if they had experienced cerebral hemorrhage or stroke. Patients were required to have provided written informed consent. The treatment protocol including off-label use of BV at patients' own cost was reviewed and approved by the institutional review board.

Treatment

All patients received BV 10 mg/kg intravenously every other week, until disease progression or discontinuation by their withdrawal, grade 2 or more cerebral hemorrhage, grade 4 non-hematological toxicities, or any other condition that would make the treatment unsafe.

Patient evaluation

The response to therapy was assessed using MR imaging and neurological examination. The Macdonald criteria were employed to evaluate the MR imaging [15]. The criteria use the largest cross-sectional area of the post-contrast T1-weighted images and also take into account the steroid dose and clinical findings. We also evaluated non-contrast T1-weighted images, T2-weighted images, FLAIR images, and diffusion-weighted images. All MR examinations were carried out at 1.5 T. MR imaging was performed after the first and the third cycles of BV treatment, and images were reviewed by a neuroradiologist (K.T.).

Measurement of mean apparent diffusion coefficient ADC value of tumors

A mean ADC (mADC) value of the tumor was calculated on a terminal of the Picture Archiving and Communication System (PACS). Gadolinium-enhancing tumor contours were manually segmented on sequential post-contrast T1-weighted images, eliminating non-enhancing regions within the tumor, and the same segmented areas were selected on the corresponding ADC maps, thereby obtaining a mADC value (10^{-6}mm^2/s) and an area (mm^2) of the tumor in each image (Fig. 1). The mADC value of the image slice was multiplied by the area to produce a total ADC value of

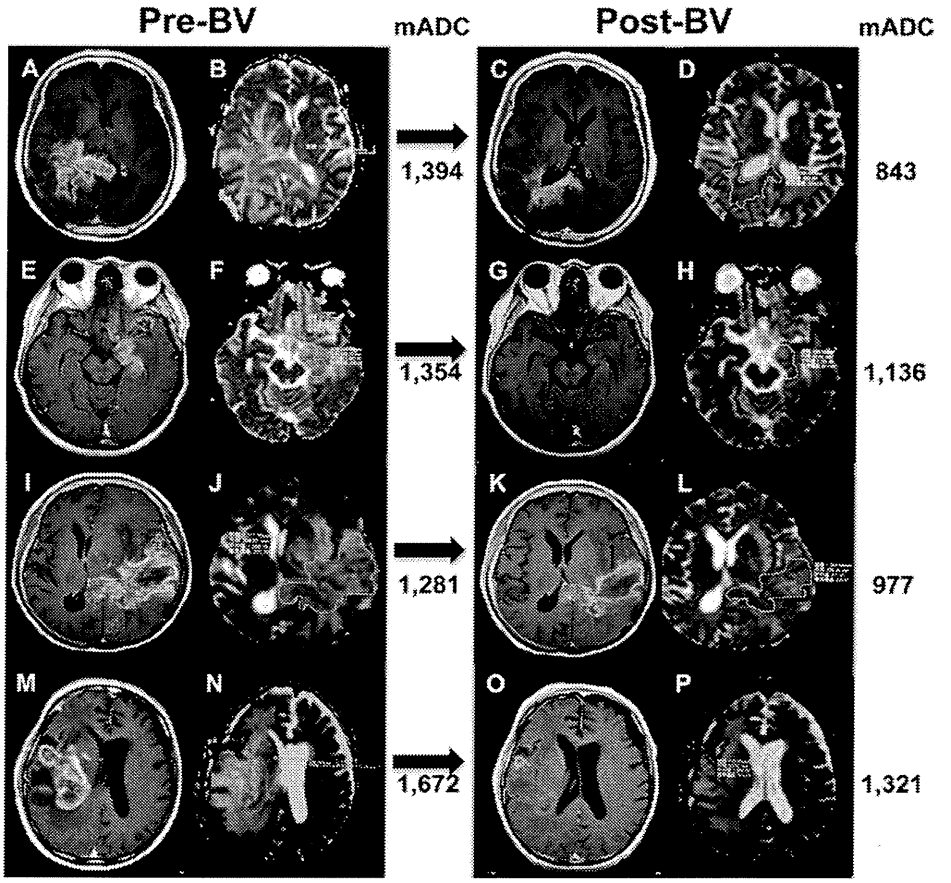

Fig. 1 Postcontrast T1-weighted images aligned side-by-side with the corresponding ADC maps of both pre- (*left-hand column*) and post-treatment (*right-hand column*) with BV in representative patients who achieved immediate response after a single BV administration. The mADC values of the lesions of interest are indicated at the *right margin* of the ADC maps. Each mADC value is calculated as described in "Patients and methods." Note that all pretreatment mADC values are above 1100 (10^{-6} mm^2/s), which subsequently decrease after BV treatment. **a, b, c, d**: case 1; **e, f, g, h**: case 2; **i, j, k, l**: case 8; **m, n, o, p**: case 9

the slice. The sum of the total ADC value of all slices for a lesion was divided by the sum of areas of all slices to achieve the net mADC value of the single enhancing lesion.

Immunohistochemistry

Immunohistochemistry analysis of surgical specimens of the original tumors entailed: (1) fixation with 10 % buffered formalin, and embedding in paraffin; (2) deparaffinizing 5-μm-thick sections of the tissues in xylene, and rehydration in 90, 70, and 50 % ethanol; (3) antigen retrieval, by autoclaving in buffered citrate (pH 7.0) at 120 °C for 10 min; (4) incubation with the primary antibody, anti-VEGF antibody (code SC-152, Santa Cruz, CA, USA) at room temperature for approximately 12 h; and (5) detection of immunoreactivity using the EnVision system (Dako, Carpinteria, CA, USA), followed by hematoxylin counterstaining.

O^6-methylguanine-DNA methyltransferase (*MGMT*) status

Methylation status of the *MGMT* gene promoter region in tumors was determined by the methylation-specific polymerase chain reaction as described elsewhere [16].

Statistical analysis

The correlation of the mADC value with response to BV was evaluated by Fisher's exact test and the Mann–Whitney *U* test. The change of mADC values before and after the first BV treatment was assessed by a paired *t* test. PFS and OS were calculated according to the Kaplan–Meier method, and differences in progression and survival according to mADC values were evaluated with the log-rank test. All the probability values were two-sided, and all statistical analyses were done at a significance level of $p = 0.05$, using the statistical package SPSS 17.0J (SPSS, Inc., Chicago, IL, USA).

Results

Bevacizumab treatment of patients with recurrent HGG after TMZ failure

From August 2009 to December 2010, nine eligible patients with recurrent or progressive HGGs (seven with GBM and two with anaplastic astrocytoma) were treated with BV monotherapy. The average patient age was 57

years (range, 22–78), and median Karnofsky Performance Scale (KPS) was 70 (30–80) (Table 1). Five patients underwent RT plus concomitant TMZ at the initial therapy, and others received TMZ monotherapy on disease progression. BV treatment was primarily (67 %) given as the second line therapy (range 2–5). The cycles of BV therapy ranged from 1 to 21 (median 7). There were no serious adverse events in any of the patients.

Response to BV

After the first BV cycle, early post-treatment MR imaging (taken between days 3 and 21, median 13) demonstrated rapid shrinkage of both enhancing and T2-elongated (hyperintense on T2-weighted and FLAIR images) areas in most tumors (Fig. 1). By a patient-based analysis, single BV treatment resulted in a decrease in evaluable enhancing tumor volume in eight of nine cases (88.9 %) (Table 1). Four patients (44.4 %) had a partial response (PR), four had a stable disease (SD), and one had a progressive disease (PD) by the Macdonald criteria; the overall response rate was 44.4 %. In cases 1, 3, and 8, both hemiparesis and disturbance of consciousness recovered soon after the first BV administration with a marked reduction of extent of hyperintensity on T2-weighted or FLAIR images along with the enhancing tumor shrinkage. KPS improved immediately in four cases (44.4 %).

Association of tumor mADC values with the response to BV

Of 15 individual evaluable enhancing lesions in the nine patients, 11 tumors shrank (Fig. 1), while four did not respond upon initial BV treatment (Fig. 2). We then evaluated parameters obtained in the MR images to determine if there were any predictors for tumor response to BV. The pretreatment MR images were obtained on days −1 to −25 (median −10). The average pretreatment mADC value for all lesions was 1249 (10^{-6} mm^2/s) (range 964–1672). Tumor mADC values were above 1100 in all of the responding tumors, in contrast to those in all non-responding lesions that scored below 1100 (Fisher's exact test, $p = 0.001$) (Fig. 3), suggesting that a pretreatment mADC value higher than 1100 may be predictive for a rapid shrinkage of enhancing tumors. Interestingly, the tumor mADC values decreased significantly after the first BV treatment in all lesions except for one that did not respond (paired t test, $p < 0.001$) (Fig. 4). The average mADC value after the first cycle of BV was 1051 (range 828–1320).

To determine whether the mADC value after the first BV treatment (post-BV mADC) could also predict a further response of the lesion to additional cycles of BV, the ratio

Table 1 Summary of cases treated with bevacizumab monotherapy on temozolomide failure

No	Age (years)	Gender	KPS (pre-BV)	Pathological Dx	RT (Gy)	TMZ cycles	TMZ OR	*MGMT* status	BV line[a]	BV cycles	Months from last RT	mADC (pre-BV) (10^{-6} mm^2/s)	Total TV (ml) (pre-BV)	BV OR	Relative TV[b]	KPS (post 1st BV)	Relapse	PFS (months)	Out-come	OS (months)
1	74	Female	40	AA	60	46	CR	nd	3	7	77	1394	61.7	SD	0.63	50	+	2.2	D	5.7
2	51	Male	70	AA	60 + SRT	14	SD	nd	2	21	15.2	1354	45.0	PR	0.03	70	+	7.7	D	16.0
3	60	Female	70	GBM	60 + SRT	11	SD	M	2	4	5.6	964–1490[c]	25.7	SD	0.88	90	+	1.5	D	3.3
4	32	Female	70	GBM-s	50	10	SD	M	3	8	35.8	1190	23.7	SD	0.73	70	+	2.3	D	5.5
5	22	Male	80	GBM-s	60	1	PD	U	2	12	2.1	1273	16.8	PR	0.13	80	+	5.5	D	10.3
6	73	Female	60	GBM	60	5	SD	U	2	1	6.7	1009–1281[c]	7.9	PD	1.78	50	+	0.4	D	3.9
7	58	Female	80	GBM	60	8	SD	U	2	8	7.6	1323	8.4	PR	0.67	80	+	3.9	D	11.1
8	51	Female	30	GBM	60 + SRT	40	CR	M	5[a]	5	4.3	1281	152.8	SD	0.54	50	+	1.4	D	2.9
9	78	Male	30	GBM	40	1	PD	U	2	3	1.9	1257–1672[c]	72.9	PR	0.24	40	+	2.1	D	8.3

KPS Karnofsky Performance Scale, *Dx* diagnosis, *RT* radiotherapy, *TMZ* temozolomide, *OR* objective response, *MGMT* O^6-methylguanine-DNA methyltransferase, *BV* bevacizumab, *mADC* mean apparent diffusion coefficient, *pre-BV* before the first BV treatment, *TV* tumor volume, *PFS* progression-free survival, *OS* overall survival, *AA* anaplastic astrocytoma, *GBM* glioblastoma, *GBM-s*, secondary GBM, *SRT* stereotactic radiotherapy, *CR* complete response, *PR* partial response, *SD* stable disease, *PD* progressive disease, *nd* not determined, *M* methylated promoter, *U* unmethylated promoter, *D*, dead

[a] Previous chemotherapy included bevacizumab

[b] The ratio of tumor volume at the first MR imaging post-bevacizumab treatment compared with that of the baseline

[c] The lowest and highest values of multiple lesions

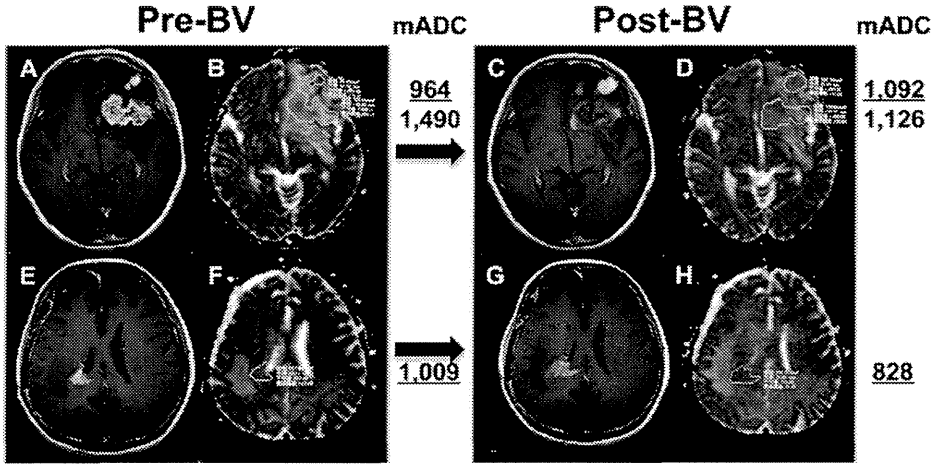

Fig. 2 Post-contrast T1-weighted images aligned side-by-side with the corresponding ADC maps in patients with tumors which did not respond to BV (**a, b, c, d**: case 3; **e, f, g, h**: case 6). Note that the non-responding lesions have mADC values below 1100 (10^{-6} mm^2/s). In case 3, the anterior frontal lesion with an initial mADC of 964 continues to grow, whereas the posterior frontal lesion that has undergone stereotactic radiotherapy before further progression shows an initial mADC of 1490 and its enhancement reduces after BV treatment

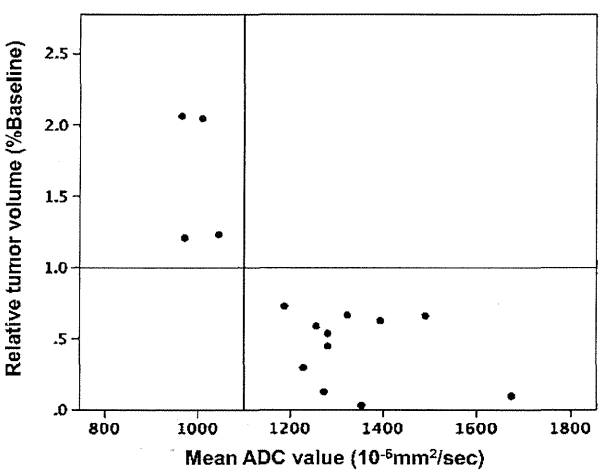

Fig. 3 Clear correlation between mean ADC values and changes in tumor size after a single BV treatment in recurrent high-grade glioma lesions. All lesions with mADC above 1100 (10^{-6} mm^2/s) shrink, while those with lower mADC continue growth (Fisher's exact test, $p = 0.001$)

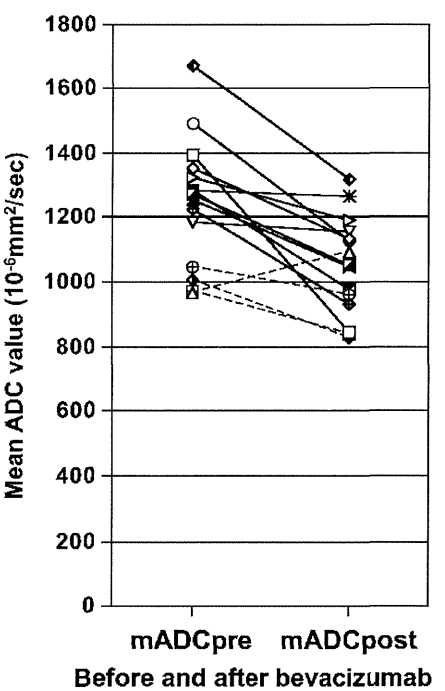

Fig. 4 Changes in mADC value between pre- and post-treatment with BV. Corresponding mADC value points of each lesion are connected with *lines*; the responding lesions are in *solid lines* and the non-responding are in *dashed lines*. mADC values of all lesions decrease after BV except for one non-responding

of tumor volumes at the first MR imaging to those at the second MR imaging taken after 2 more BV cycles (median interval, 39 days; range, 35–56 days) was measured (Table 2). Post-BV mADC significantly correlated with response to additional BV (Mann–Whitney U test, $p = 0.045$) and all five high post-BV mADC (>1100) lesions shrank after the additional BV treatments. Although three of eight (37.5 %) low post-BV mADC (<1100) lesions also decreased in size, the majority (5/8, 62.5 %) did not respond further, which approached statistical significance (Fisher's exact test; $p = 0.075$). These observations suggest that even the mADC immediately after the first BV treatment may be of predictive value for further response to BV.

Table 2 mADC values before and after the first bevacizumab treatment and the change in tumor volume

Case	Lesion	mADC (10^{-6} mm^2/s)		TV (%baseline) (1st F/U MRI)	TV (%baseline) (2nd F/U MRI)	TV (%1st MRI) (2nd F/U MRI)
		Before	After			
1	P/T	1394.2	842.5	62.7	21.8	34.9
2	T	1353.6	1135.8	3.3	0.0	0.0
3	F	1490.1	1125.6	66.1	63.6	96.3
	F-AL	964.3	1092.0	206.4	445.5	215.9
	F-AM	971.1	841.1	120.9	135.5	112.1
	F-MF	1227.6	930.0	29.8	30.4	103.1
	F-PM	1044.5	961.8	123.2	225.6	183.1
4	F-BG	1187.5	1155.4	72.8	15.2	20.9
5	T	1272.6	1053.0	12.9	0.0	0.0
6	T	1008.9	827.6	204.6	na	na
	F	1281.1	1267.7	44.8	na	na
7	CC	1323.4	1192.9	66.5	18.3	27.9
8	PT	1280.9	977.4	53.8	106.7	198.4
9	F	1672.4	1320.5	10.0	7.3	73.7
	F	1256.7	1046.5	58.9	50.1	85.1

TV, tumor volume, *F/U* follow-up, *P* parietal, *T* temporal, *F* frontal, *AL* antero-lateral, *AM* antero-medial, *MF* mid-frontal, *PM* premotor, *BG* basal ganglia, *CC* corpus callosum

Survival

After a median follow-up of 5.7 months (range, 2.9–16.0), all patients had progressed and died despite a high rate of early response. PFS from the initiation of BV therapy was 2.2 months [95 % confident interval (CI) 1.8–2.6 months]. PFS for two patients (cases 3 and 6) having a lesion with mADC value <1100 (low mADC) was short (0.4 months), whereas PFS for others having all lesions with mADC >1100 (high mADC) was significantly longer (2.3 months, 95 % CI 2.0–2.6) (log-rank test, $p = 0.018$). Median OS after the start of BV treatment was 5.7 months (95 % CI 5.1–6.2). Patients having all lesions with a high mADC (>1100) survived significantly longer (median 8.3 months, 95 % CI 1.4–15.2) than those with a low mADC tumor(s) (median 3.3 months, $p = 0.046$), despite the small sample number (9 cases). The tumor volume of enhancing lesions prior to initiation of BV was not associated with either PFS or OS (Table 1, data not shown).

VEGF expression in the original tumor specimens

Immunohistochemistry staining of VEGF-A was performed in the primary tumors and all but one were found to express VEGF to a variable extent (data not shown). Expression at the beginning of BV treatment was not determined due to lack of re-resection prior to BV therapy. The tumor with negative VEGF staining (case 6) did not respond to BV.

Relationship of mADC with *MGMT* promoter methylation status

While *MGMT* status is prognostic/predictive for survival in GBM patients [17, 18], tumoral mADC values were not associated with *MGMT* methylation status (Fisher's exact test; $p = 0.445$) in the seven GBM cases (Table 1). Taken together, while we observed that response of recurrent lesions after a single dose of BV was significantly correlated with a mean ADC value of the tumors above 1100 (10^{-6}mm^2/s), it was not with VEGF expression or *MGMT* status.

Discussion

Although BV has shown efficacy against TMZ-refractory GBMs, some tumors may also be resistant to BV, progressing to fatality [19], and thus determining their sensitivity to BV prior to initiation of the treatment could have significant clinical value. Here, we demonstrated that the pretreatment mADC value of enhancing tumors was predictive for initial response to BV monotherapy in recurrent HGGs. All lesions with the mADC above 1100 (10^{-6} mm^2/s) responded, in clear contrast to those with the mADC below 1100, which did not respond ($p = 0.001$) (Fig. 3). The mADC values decreased after the first BV treatment in all lesions, except for one that did not respond. The second mADC value obtained after the first BV treatment was also a good indicator for further response to additional BV when it remained above 1100 ($p = 0.045$). Furthermore, the high mADC value also significantly correlated with elongation of both PFS and OS after BV treatment in patients with TMZ-refractory recurrent HGGs.

Anti-VEGF therapy is expected to normalize vascular structure, capillary permeability and interstitial pressure more effectively in areas with strong edema and necrotic changes than in those with "packed" tumor cells. The ADC value represents movement of protons of water molecules and may be increased in areas where tissue edema and necrotic components have been induced by tissue damage from tumor burden and cytotoxic therapies [9–11]. This may account for our findings that glioma lesions with a high pretreatment ADC value shrank upon BV challenge whereas those with a low ADC value did not. Such non-responding lesions also tended to be strongly enhanced (e.g., a subcortical lesion in the left frontal lobe in Fig. 2a), consistent with the observation that GBMs that relapsed after BV treatment exhibited low ADC values and hyperintensity on diffusion-weighted images [20].

Pope et al. reported that PFS correlated with crude average ADC values within areas showing contrast enhancement in 41 recurrent GBM cases who underwent BV treatment. Of note, when the average ADC value of the lower peak of biphasic peaks in ADC histograms ($mADC_L$) was lower than 1201, PFS was significantly extended [21]. Our use of whole ADC values within an enhancing tumor to calculate a mean value on a PACS terminal in clinics without specific software successfully segregated responding from non-responding lesions. This simple method might incorporate regions of extremely high ADC values containing necrotic tissues, resulting in a shift of the mean value toward a higher value, compared with the histogram-based analysis. However, regions exhibiting apparent necrosis or cyst could be readily excluded when defining a tumor on each ADC map, in order to avoid such data contamination. We also eliminated T2-elongated areas surrounding contrast-enhancing lesions because they may contain both edematous white matter and non-enhancing tumor to a variable extent. As a result, our data show clear segregation of lesions for response by ADC value at 1100 (10^{-6} mm^2/s), smaller than the cut-off value of 1201 in the Pope study [21]. It would be beneficial in daily practice to use this simple measurement, as it does not require specific histogram analysis, though it needs further accumulation of cases for validation.

Conflicting findings that BV induces rapid shrinkage of the enhancing lesions while they subsequently regrow in a relatively short term might represent, at least partly, the recently recognized "pseudo-response," a decrease in enhancing tumor on MR imaging without a decrease in tumor activity [22]. This has been reported in a clinical trial where radiation necrosis was successfully treated with BV [23]. To date, there are no validated imaging methods to determine whether the observed shrinkage of areas of contrast enhancement were due to real tumor reduction or pseudo-response, as well as progression without an emergence or increase of enhancing lesion [24]. Indeed, the potential value of changes in T2 relaxation time is recently suggested by an observation that an elevated residual, post-treatment, median T2 may be predictive of both PFS and OS [25]. Efforts to clarify these issues include application of the newly-developed response criteria, Response Assessment in Neuro-Oncology (RANO), utilizing elongation of T2 relaxation time as a surrogate for non-enhancing tumor [26], and MR imaging techniques such as MR perfusion studies that are under investigation in large trials for validity. In our study, there were two patients (cases 3 and 8) who underwent stereotactic RT on recurrence prior to BV initiation, and one patient (case 5) who received BV within 3 months after completion of induction-concomitant RT plus TMZ. Two of these three patients had a PR by single BV treatment with further progression in 2 and 5.5 months, indicating no clear relationship between response and potential radiation injury.

A recent study reported that the lower ADC_L value rather correlated with longer PFS for patients with newly-diagnosed GBM [27], in contrast to recurrent GBM. It also showed an association between ADC values and *MGMT* methylation status [27], which was not observed in our series. Whether this association might be influenced by the difference of tumor microstructure in the setting of newly-diagnosed or treatment-modified recurrent tumors needs to be clarified.

Limitations of our study include the small number of patients and lesions analyzed, heterogeneous prior treatment regimens applied in some patients, and specimens from primary newly-diagnosed tumors used for determination of VEGF and *MGMT* status. This might hamper drawing definite conclusions about the relationship of the mADC value with survival gain or VEGF/*MGMT* status, as well as analyzing whether pathological findings of treated tumors may also correlate with either mADC values or responsiveness to BV, or both. However, even with the small sample size, a clear segregation of responders from non-responders and survival prediction were seen using our simplified mADC measurement and this warrants further investigation in a larger series.

Conclusions

Bevacizumab monotherapy is an active regimen for patients with TMZ-refractory recurrent gliomas leading to rapid lesion shrinkage, and the tumor mADC value can be a useful marker for prediction of BV response and survival, and thus for patient selection. It would be also intriguing to investigate methods of delineating tumors in which BV would provide long-term response in the future.

Acknowledgments This work was supported partially by grants of the Ministry of Health, Labour, and Welfare of Japan (H20-ganrinsyou-ippan-019 and 20shi-4) (to MN). We thank Kuninori Kobayashi, RT (Radiology Section, Kyorin University Hospital) for obtaining MR imaging data.

Conflict of interest The authors declare that they have no conflict of interest.

References

1. Stupp R, Mason WP, van den Bent MJ et al (2005) Radiotherapy plus concomitant and adjuvant temozolomide for glioblastoma. N Engl J Med 352:987–996
2. Norden AD, Drappatz J, Wen PY (2009) Antiangiogenic therapies for high-grade glioma. Nat Rev Neurol 5:610–620

3. Fischer I, Gagner JP, Law M et al (2005) Angiogenesis in gliomas: biology and molecular pathophysiology. Brain Pathol 15:297–310
4. Yuan F, Chen Y, Dellian M et al (1996) Time-dependent vascular regression and permeability changes in established human tumor xenografts induced by an anti-vascular endothelial growth factor/vascular permeability factor antibody. Proc Natl Acad Sci USA 93:14765–14770
5. Chamberlain MC (2010) Emerging clinical principles on the use of bevacizumab for the treatment of malignant gliomas. Cancer 116:3988–3999
6. Vredenburgh JJ, Desjardins A, Herndon JE 2nd et al (2007) Bevacizumab plus irinotecan in recurrent glioblastoma multiforme. J Clin Oncol 25:4722–4729
7. Friedman HS, Prados MD, Wen PY et al (2009) Bevacizumab alone and in combination with irinotecan in recurrent glioblastoma. J Clin Oncol 27:4733–4740
8. Kreisl TN, Kim L, Moore K et al (2009) Phase II trial of single-agent bevacizumab followed by bevacizumab plus irinotecan at tumor progression in recurrent glioblastoma. J Clin Oncol 27:740–745
9. Sugahara T, Korogi Y, Kochi M et al (1999) Usefulness of diffusion-weighted MRI with echo-planar technique in the evaluation of cellularity in gliomas. J Magn Reson Imaging 9:53–60
10. Mardor Y, Roth Y, Ochershvilli A et al (2004) Pretreatment prediction of brain tumors' response to radiation therapy using high b-value diffusion-weighted MRI. Neoplasia 6:136–142
11. Chenevert TL, Sundgren PC, Ross BD (2006) Diffusion imaging: insight to cell status and cytoarchitecture. Neuroimaging Clin N Am 16:619–632 viii-ix
12. Oh J, Henry RG, Pirzkall A et al (2004) Survival analysis in patients with glioblastoma multiforme: predictive value of choline-to-*N*-acetylaspartate index, apparent diffusion coefficient, and relative cerebral blood volume. J Magn Reson Imaging 19:546–554
13. Murakami R, Sugahara T, Nakamura H et al (2007) Malignant supratentorial astrocytoma treated with postoperative radiation therapy: prognostic value of pretreatment quantitative diffusion-weighted MR imaging. Radiology 243:493–499
14. Higano S, Yun X, Kumabe T et al (2006) Malignant astrocytic tumors: clinical importance of apparent diffusion coefficient in prediction of grade and prognosis. Radiology 241:839–846
15. Macdonald DR, Cascino TL, Schold SC Jr et al (1990) Response criteria for phase II studies of supratentorial malignant glioma. J Clin Oncol 8:1277–1280
16. Nagane M, Nozue K, Shimizu S et al (2009) Prolonged and severe thrombocytopenia with pancytopenia induced by radiation-combined temozolomide therapy in a patient with newly diagnosed glioblastoma—analysis of O^6-methylguanine-DNA methyltransferase status. J Neurooncol 92:227–232
17. Hegi ME, Diserens AC, Gorlia T et al (2005) MGMT gene silencing and benefit from temozolomide in glioblastoma. N Engl J Med 352:997–1003
18. Nagane M, Kobayashi K, Ohnishi A et al (2007) Prognostic significance of O6-methylguanine-DNA methyltransferase protein expression in patients with recurrent glioblastoma treated with temozolomide. Jpn J Clin Oncol 37:897–906
19. Wong ET, Brem S (2008) Antiangiogenesis treatment for glioblastoma multiforme: challenges and opportunities. J Natl Compr Canc Netw 6:515–522
20. Gerstner ER, Frosch MP, Batchelor TT (2010) Diffusion magnetic resonance imaging detects pathologically confirmed, nonenhancing tumor progression in a patient with recurrent glioblastoma receiving bevacizumab. J Clin Oncol 28:e91–e93
21. Pope WB, Kim HJ, Huo J et al (2009) Recurrent glioblastoma multiforme: ADC histogram analysis predicts response to bevacizumab treatment. Radiology 252:182–189
22. Brandsma D, van den Bent MJ (2009) Pseudoprogression and pseudoresponse in the treatment of gliomas. Curr Opin Neurol 22:633–638
23. Levin VA, Bidaut L, Hou P et al (2011) Randomized double-blind placebo-controlled trial of bevacizumab therapy for radiation necrosis of the central nervous system. Int J Radiat Oncol Biol Phys 79:1487–1495
24. Pope WB, Young JR, Ellingson BM (2011) Advances in MRI assessment of gliomas and response to anti-VEGF therapy. Curr Neurol Neurosci Rep 11:336–344
25. Ellingson BM, Cloughesy TF, Lai A et al (2012) Quantification of edema reduction using differential quantitative T2 (DQT2) relaxometry mapping in recurrent glioblastoma treated with bevacizumab. J Neurooncol 106:111–119
26. Wen PY, Macdonald DR, Reardon DA et al (2010) Updated response assessment criteria for high-grade gliomas: response assessment in neuro-oncology working group. J Clin Oncol 28:1963–1972
27. Pope WB, Lai A, Mehta R et al (2011) Apparent diffusion coefficient histogram analysis stratifies progression-free survival in newly diagnosed bevacizumab-treated glioblastoma. AJNR Am J Neuroradiol 32:882–889

Epilepsy & Behavior Case Reports 1 (2013) 97–105

Contents lists available at SciVerse ScienceDirect

Epilepsy & Behavior Case Reports

journal homepage: www.elsevier.com/locate/ebcr

Case Report

Epilepsy surgery of dysembryoplastic neuroepithelial tumors using advanced multitechnologies with combined neuroimaging and electrophysiological examinations ☆

Jun Shinoda [a,*], Kazutoshi Yokoyama [a], Kazuhiro Miwa [a], Takeshi Ito [a], Yoshitaka Asano [a], Shingo Yonezawa [a], Hirohito Yano [b]

[a] Chubu Medical Center for Prolonged Traumatic Brain Dysfunction and Section of Neurosurgery, Kizawa Memorial Hospital, Department of Clinical Brain Sciences, Gifu University Graduate School of Medicine, Japan
[b] Department of Neurosurgery, Gifu University Graduate School of Medicine, Japan

ARTICLE INFO

Article history:
Received 12 June 2013
Accepted 13 June 2013
Available online xxxx

Keywords:
Dysembryoplastic neuroepithelial tumor
Epilepsy
Positron emission tomography
Electrocorticography
Magnetoencephalography
Tractography

ABSTRACT

Purpose: We report three cases of dysembryoplastic neuroepithelial tumor (DNT) with intractable epilepsy which were successfully treated with surgery.
Methods: In all cases, technology beyond the routine workup was critical to success. Preoperative magnetic resonance imaging, ^{18}F-fluorodeoxyglucose positron emission tomography (PET), ^{11}C-methionine-PET, interictal electroencephalography, and intraoperative electrocorticography were utilized in all patients. In individual cases, however, additional procedures such as preoperative magnetoencephalography (Case 1), diffusion tensor fiber tractography, a neuronavigation system, and intraoperative somatosensory-evoked potential (Case 2), and fiber tractography and the neuronavigation-guided fence-post tube technique (Case 3) were instrumental.
Results: In all the cases, the objectives of total tumor resection, resection of the epileptogenic zone, and complete postoperative seizure control and the avoidance of surgical complications were achieved.
Conclusions: Dysembryoplastic neuroepithelial tumor is commonly associated with medically intractable epilepsy, and surgery is frequently utilized. As DNT may arise in any supratentorial and intracortical locations within or near the critical area of the brain, meticulous surgical strategies are necessary to avoid neurological deficits. We demonstrate in the following three cases how adjunct procedures using advanced multitechnologies with neuroimaging and electrophysiological examinations may be utilized to ensure success in DNT surgery.

1. Introduction

Dysembryoplastic neuroepithelial tumor (DNT), first described by Daumas-Duport et al. [1], is, under the current World Health Organization (WHO) classification, a low-grade glioneuronal tumor causing intractable complex partial seizures [2]. Complete resolution of seizures in a large percentage of both adult and pediatric patients is achieved with surgery [3–8]. Though the primary objective of surgery is complete seizure control without anticonvulsant therapy, the prevention of recurrent disease and the diagnosis of malignant transformation are also goals of surgical resection [9]. The widespread surgical treatment of epilepsy due to DNT has, however, been criticized because surgery carries a nonnegligible risk of surgical sequelae including neurological, cognitive, and neuropsychological impairment. Guidelines regarding the preoperative evaluation and intraoperative determination of the extent of resection have not been standardized. Magnetic resonance imaging (MRI), ^{11}C-methionine positron emission tomography (MET-PET), and ^{18}F-fluorodeoxyglucose (FDG)-PET are routinely used at our institution preoperatively to assess the morphology and metabolism of brain tumors with epileptogenicity in addition to interictal electroencephalography (EEG). Additionally, electrocorticography (ECoG) is also used intraoperatively to detect the epileptogenic zone (EZ).

We report three cases of DNT with intractable epilepsy, successfully treated with surgery, in which not only imaging functional studies but also advanced neurosurgical technologies were critical for planning and supported the role for surgery. These interventions included preoperative magnetoencephalography (MEG) (Case 1), fiber tractography obtained from diffusion tensor imaging (DTI), a neuronavigation system, and intraoperative somatosensory evoked potential (SEP) (Case 2) and fiber tractography and the neuronavigation-guided fence-post tube technique (Case 3) (Table 1).

The medical equipment used in these cases were MRI (Signa, GE Healthcare, Milwaukee, Wisconsin, USA and Achieva 3.0 T, Philips,

* Corresponding author at: Chubu Medical Center for Prolonged Traumatic Brain Dysfunction and Section of Neurosurgery, Kizawa Memorial Hospital, Department of Clinical Brain Sciences, Gifu University Graduate School of Medicine, 630 Shino-kobi, Kobi-cho, Minokamo, Gifu 505-0034, Japan. Fax: +81 574 24 2230.
E-mail address: junshino@joy.ocn.ne.jp (J. Shinoda).

2213-3232/$ – see front matter © 2013 The Authors. Published by Elsevier Inc. All rights reserved.
http://dx.doi.org/10.1016/j.ebcr.2013.06.002

Table 1
Clinical summary of the three cases of DNT.

Case no.	Age (years)	Sex	Preoperative duration of epilepsy	Tumor location	Tumor size (cm)	ME used preope.	ME used intraoperatively	Surgery	Extent of tumor resection	Surgical complications	Engel class
1	43	F	20 years	Left temporal lobe	1.8 × 1.8 × 1.8	MRI EEG MET-PET FDG-PET MEG	ECoG	First	Total	None	I
2	5	F	4 months	Left frontal lobe	3.0 × 3.0 × 4.0	MRI EEG MET-PET FDG-PET TG	ECoG SEP NNS	First	Total	None	I
3	10	F	4 years	Left temporal lobe	6.5 × 5.0 × 4.0	MRI EEG MET-PET FDG-PET TG	ECoG NNGFPT	Second	Total	None	I

ME = medical equipment; MRI = magnetic resonance imaging; EEG = electroencephalography; MET-PET = ^{11}C-methionine positron emission tomography; FDG-PET = ^{18}F-fluorodeoxyglucose positron emission tomography; MEG = magnetoencephalography; TG = tractography; ECoG = electrocorticography; SEP = somatosensory-evoked potential; NNS = neuronavigation system; NNGFPT = neuronavigation-guided fence-post tube technique.

The Netherlands), PET (GE, Yokokawa Medical System, Hino, Tokyo, Japan and Eminence Stargate, Shimadzu, Kyoto, Japan), neuronavigation system (VectorVision, BrainLab, Munchen, Germany), SEP/EEG/ECoG (Neuropack X1, Nihonkohden, Tokyo, Japan), and MEG (Elekta Neuromag, Helsinki, Finland). Magnetoencephalography in Case 1 was performed at Komaki City Hospital.

2. Case report

2.1. Case 1

The patient, a 43-year-old woman, presented with a 20-year history of complex partial seizures occasionally followed by generalized tonic–clonic convulsive seizures. Despite treatment for over two years with multiple anticonvulsants, she continued to have seizures several times a month. Her MRI showed a relatively well-demarcated, small, mass lesion (1.8 × 1.8 × 1.8 cm) in the left medial temporal lobe, which presented with hypointensity on a T1-weighted image (T1WI), hyperintensity on T2WI, hypointensity with a surrounding high intensity ring in fluid attenuated inversion recovery (FLAIR), no gadolinium (Gd) enhancement, low uptake in MET-PET, and hypo-uptake in FDG-PET (Figs. 1A, B, C, and D). Preoperative interictal EEG did not show any significant epileptogenic activity. Preoperative interictal MEG, however, showed clustered dipoles in the region lateral to the tumor (Figs. 1E and F). A combined total tumor resection and left anterior temporal lobectomy was performed. Intraoperative ECoG monitoring was used to verify complete resection of the EZ, which was defined as the peritumoral region with interictal spikes on the intraoperative ECoG (Figs. 1G and H, 2A and B). Epileptiform discharges, which emerged on ECoG before resection of

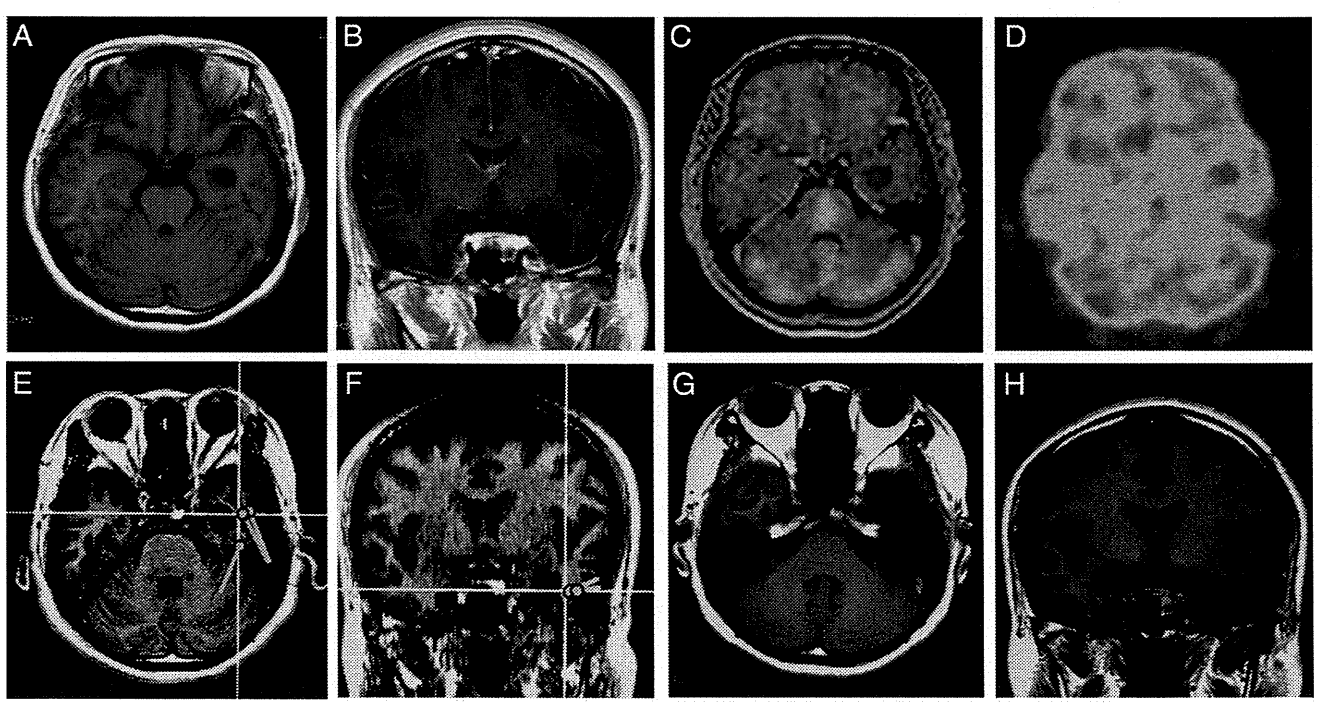

Fig. 1. Case 1. T1WI showing a relatively well-demarcated, small hypointensity mass lesion in the left medial temporal lobe in axial (A) and coronal (B) images. The tumor shows low uptake in MET-PET (fused with T1WI) (C) and hypo-uptake in FDG-PET (D). Preoperative interictal MEG shows clustered dipoles in the region lateral to the tumor (E and F). Postoperative T1WI showed the tumor to be totally resected (G and H).

the lesion, disappeared after lesion resection (Figs. 2C and D). There were no surgical complications. The tumor was histologically diagnosed as a DNT. The patient was continued on anticonvulsants for 12 months postoperatively. Following cessation of the anticonvulsants, she remained seizure-free as of nine years following surgery. Postoperative interictal EEGs have not shown any significant epileptogenic activity (Engel class I [9]).

2.2. Case 2

The patient, a five-year-old girl, presented a four-month history of complex partial seizures occurring a few times a day. Anticonvulsants reduced the seizure frequency to a few times a week. Her MRI showed a relatively well-demarcated mass lesion (3.0 × 3.0 × 4.0 cm) in the left frontal lobe extending to the left lateral ventricle wall, which

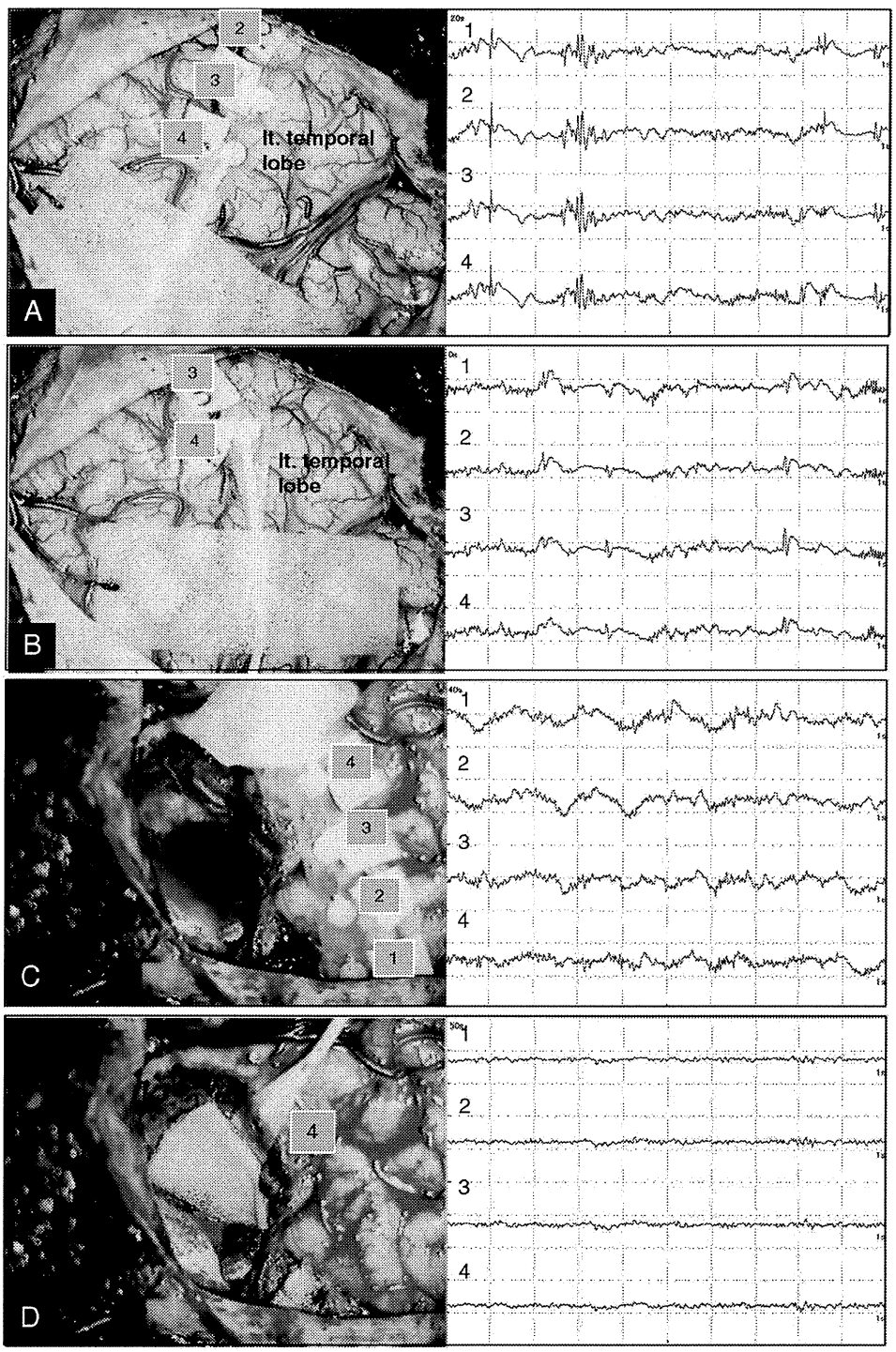

Fig. 2. Case 1. Intraoperative ECoG prior to lesion resection showing interictal spikes, with representative ECoGs shown from different two sites (A and B). Epileptiform discharges which emerged on ECoG before lesion resection disappeared after lesion resection as shown on representative ECoGs from two different sites (C and D).

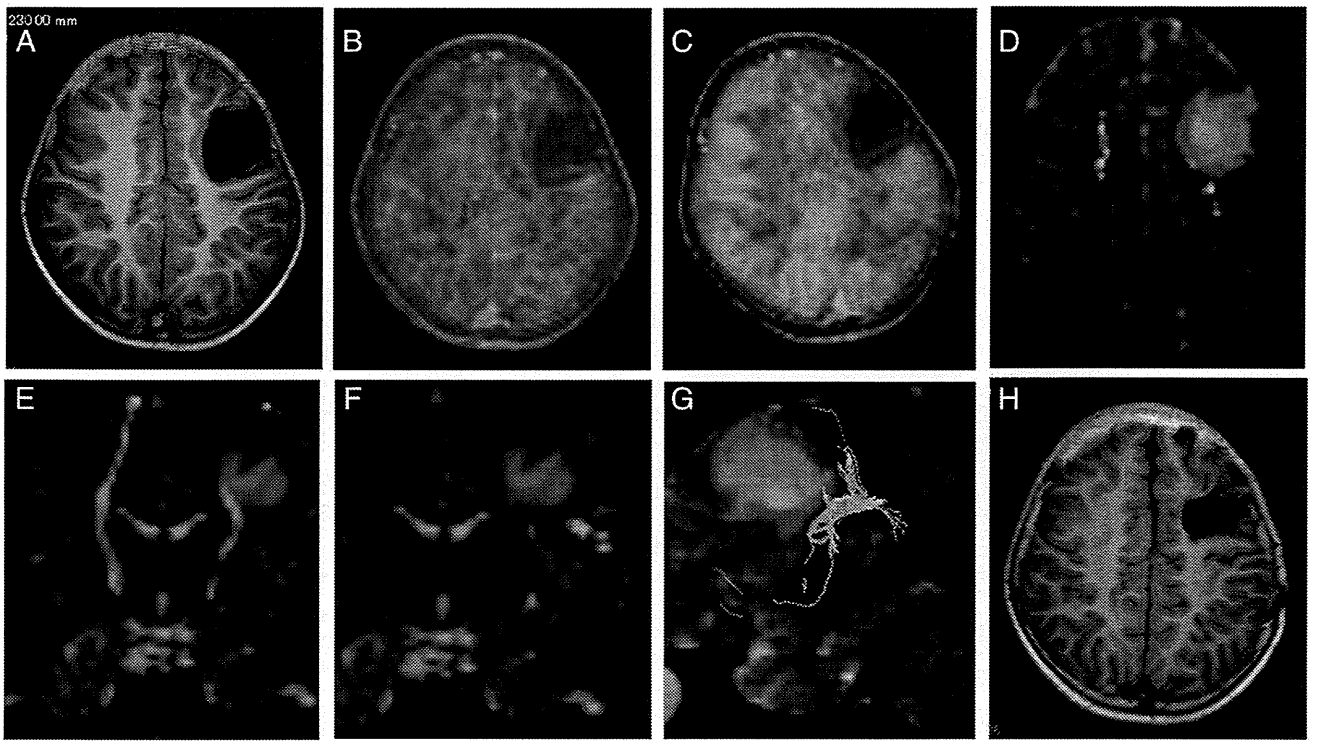

Fig. 3. Case 2. T1WI showing a well-demarcated hypointensity mass lesion in the left frontal lobe (A). The tumor shows low uptake in MET-PET (fused with T1WI) (B) and hypo-uptake in FDG-PET (fused with T1WI) (C). Fiber tractography showing that the left pyramidal tract is located posteromediocaudal to the tumor (D and E) and that the left arcuate fasciculus is located caudolateral to the tumor (F and G). Postoperative T1WI showed the tumor to be totally resected (H).

presented with hypointensity on T1WI, hyperintensity on T2WI, hypointensity with a surrounding high intensity irregular ring on FLAIR, no Gd enhancement, low uptake in MET-PET, and hypo-uptake in FDG-PET (Figs. 3A, B, and C). Preoperative interictal EEG showed frequent epileptiform spike discharges on the left frontal region. Fiber tractography showed that the left pyramidal tract lay just posteromediocaudal to the tumor (Figs. 3D and E) and that the left arcuate fasciculus lay just caudolateral to the tumor (Figs. 3F and G). In the surgery, at first, the left central sulcus was identified using intraoperative SEP (Fig. 4). A total tumor resection with careful resection of the EZ, which was defined as the peritumoral regions with interictal spikes on the intraoperative ECoG, was performed using a neuronavigation system under monitoring of the intraoperative ECoG (Figs. 3H, 5A and B). Epileptiform discharges, which emerged on ECoG before the lesion was resected, completely disappeared after lesion resection (Figs. 5C and D). She had no surgical complications. The tumor was histologically diagnosed as a DNT. She was continued on anticonvulsants for 12 months postoperatively. She remains seizure-free and off anticonvulsants as of her most recent follow-up three years after surgery. Her postoperative interictal EEG has not shown any significant epileptogenic activity (Engel class I [9]).

2.3. Case 3

The patient, a 10-year-old girl, presented with a history of surgery for DNT in the left posterior temporal lobe. She had developed complex

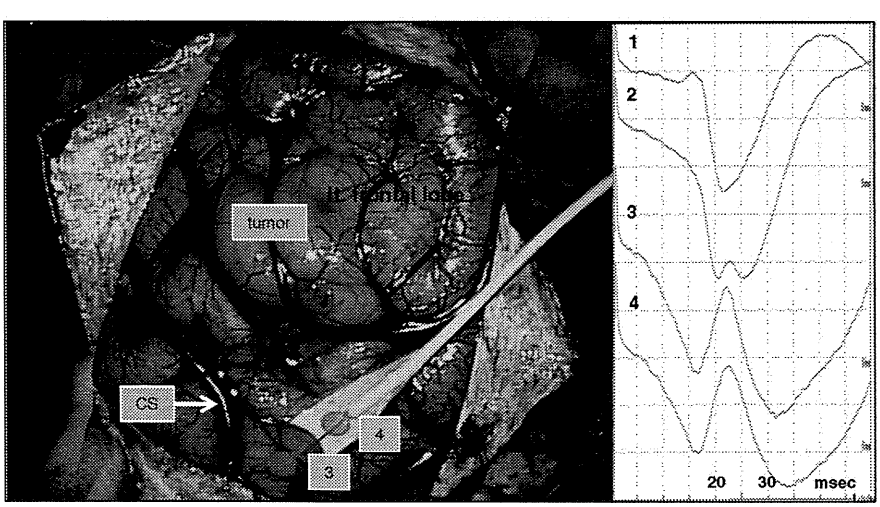

Fig. 4. Case 2. The left central sulcus was identified using intraoperative SEP. CS = central sulcus.

partial seizures refractory to anticonvulsants and had seizures a few times a month before the surgery. She underwent a partial resection of the tumor in a community hospital at the age of eight years, and the tumor was diagnosed as a DNT histologically (Fig. 6A). After surgery, she was seizure-free for 12 months on anticonvulsant medication; however, seizures recurred a few times per day. She was referred to our hospital, and her MRI showed a relatively well-demarcated mass lesion (6.5 × 5.0 × 4.0 cm) in the left posterior temporal lobe with a cavity corresponding to the prior area of resection in the posterior portion of the tumor. The tumor presented with hypointensity on T1WI, hyperintensity on T2WI, hypointensity with a surrounding irregular high intensity area in the white matter on FLAIR, and no Gd enhancement (Fig. 6B). The MRI revealed tumor progression, and the tumor intensities were the same as on the prior preoperative imaging (Figs. 6A and B). The tumor showed low uptake in MET-PET and hypo-uptake in FDG-PET (Figs. 6C and D). Preoperative interictal EEG showed frequent epileptiform spike discharges on the left occipitotemporal region. The previous surgery had resulted in right upper quadrant hemianopsia. Fiber tractography showed that the residual left visual tract lay just mediorostral to the tumor (Figs. 6E and F). We performed a complete total tumor resection with careful resection of the EZ, which was defined as the peritumoral region with interictal spikes on the

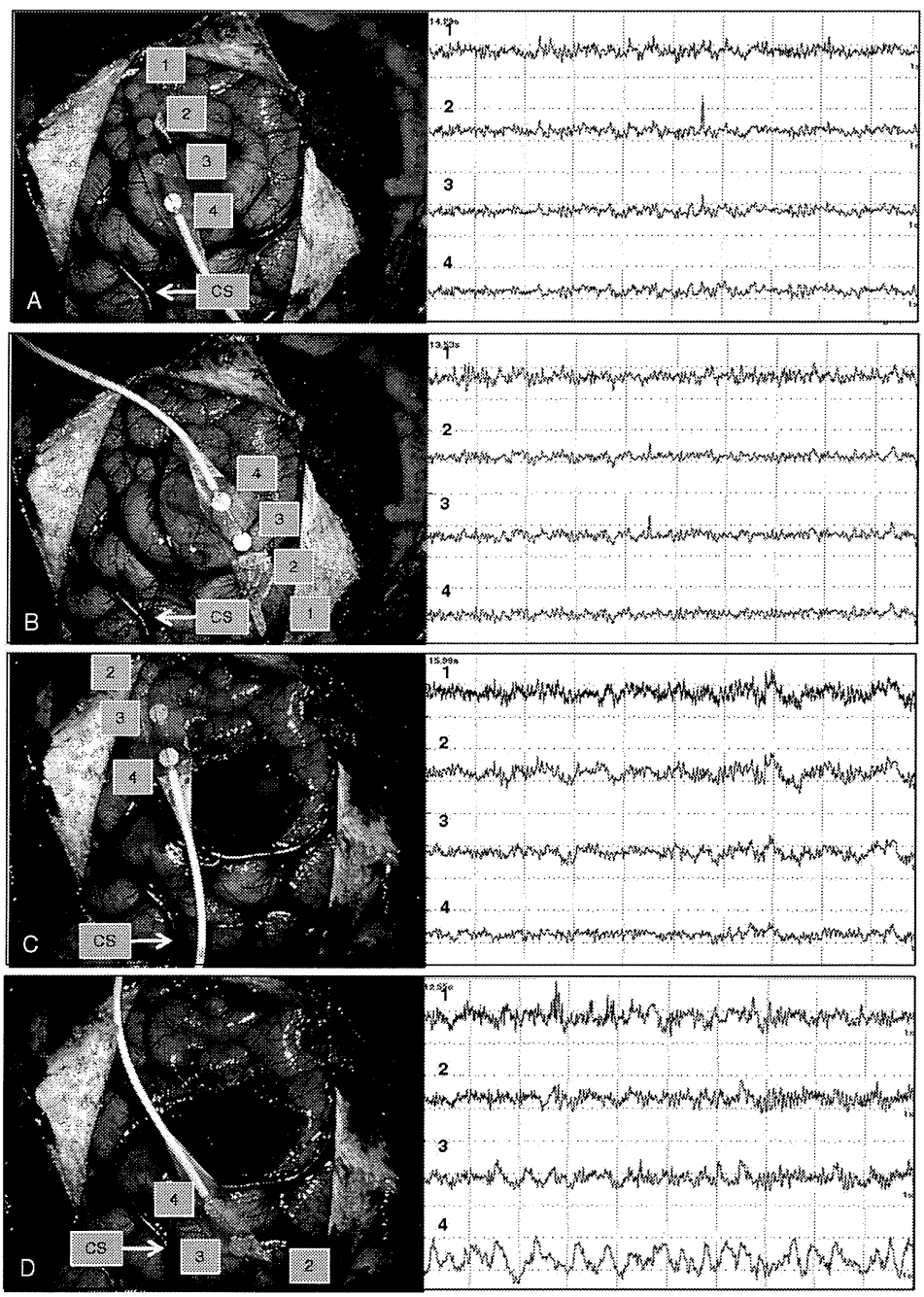

Fig. 5. Case 2. Intraoperative ECoG before the lesion resection showing interictal spikes, and the representative ECoGs from two different sites (A and B). Epileptiform discharges which emerged on ECoG before lesion resection disappeared after lesion resection, and the representative ECoGs from two different sites are shown (C and D). CS = central sulcus.

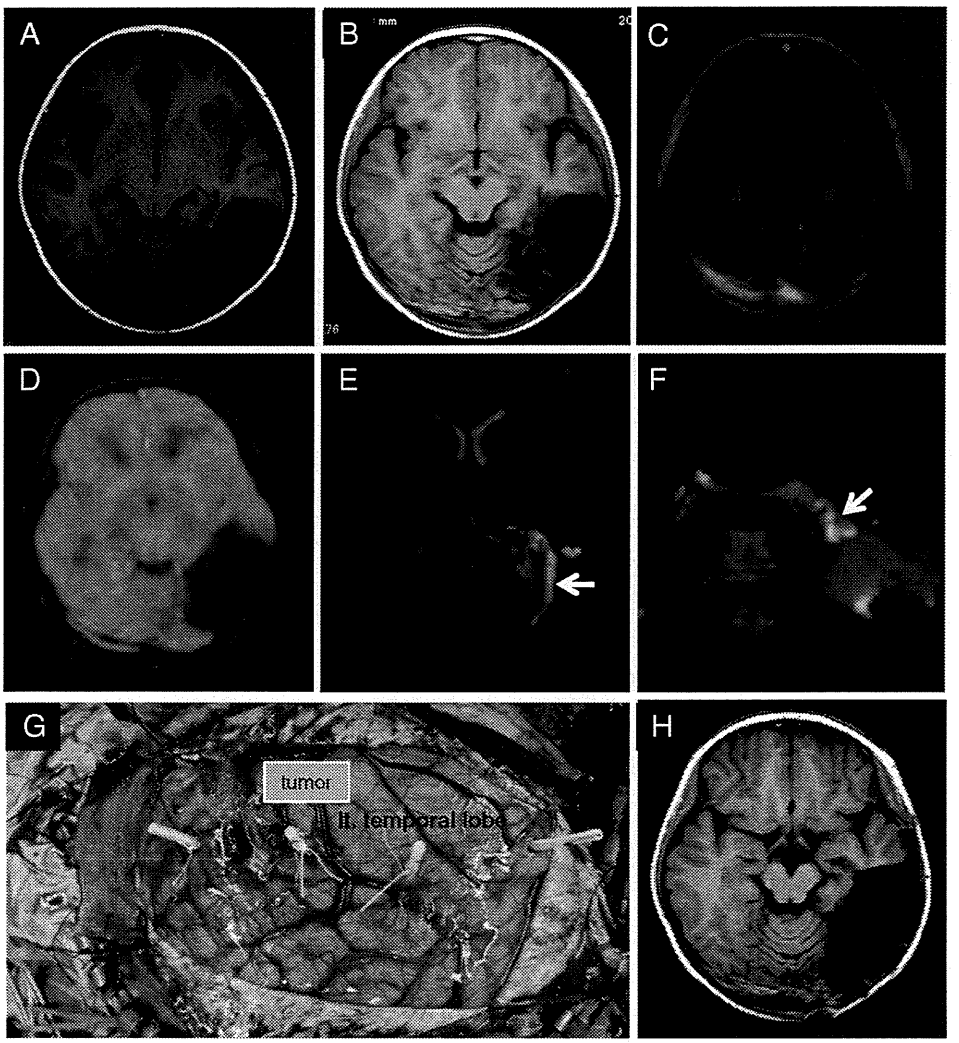

Fig. 6. Case 3. T1WI after the first surgery showing a partially resected, well-demarcated, hypointensity mass lesion in the left posterior temporal lobe (A). Two years later, T1WI showing tumor progression (B). The tumor showed low uptake in MET-PET (fused with T1WI) (C) and hypo-uptake in FDG-PET (fused with T1WI) (D). Fiber tractography showed the left visual tract (arrow) to be mediorostral to the tumor (E and F). This is a photograph showing the neuronavigation-guided fence-post tube technique used in the surgery (G). Postoperative T1WI showed that the tumor was totally resected (H).

intraoperative ECoG, using a neuronavigation-guided fence-post tube technique with monitoring of intraoperative ECoG (Figs. 6G and H, 7A and B). Epileptiform discharges which emerged on the ECoG completely disappeared after lesion resection (Fig. 7C). She had no surgical complications and exhibited no worsening of the visual field deficit. The tumor was diagnosed as a DNT histologically without malignant transformation. She was maintained on anticonvulsants and had no recurrence five months postoperatively. Postoperative interictal EEG did not show any significant epileptogenic activity (Engel class I [9]).

3. Discussion

The goals of surgery for DNT include not only complete tumor resection but also complete seizure control by resecting the EZ, while avoiding surgical sequela [10]. Imaging and functional studies are indispensable adjuncts to meticulous surgical techniques for achieving these goals. In addition to preoperative interictal EEG and MRI, preoperative FDG-PET, MET-PET, and intraoperative ECoG have been used routinely for surgical planning for resection of brain lesions with epileptogenicity such as DNT in our hospital.

Characteristics of DNT, such as a well-demarcated margin, benign clinical course, indolent biology, and the frequent association of a peritumoral EZ, are conducive to surgical management. The preoperative diagnosis of a DNT facilitates the assemblage of intraoperative monitoring equipment necessary for precisely excising the EZ. Epileptogenic brain tumors which should be differentiated from DNT include diffuse astrocytoma, oligodendroglioma, pleomorphic xanthoastrocytoma, pilocytic astrocytoma, gangliocytoma, and ganglioglioma. Some may be easily differentiated from DNT using a conventional CT and/or MRI; however, others cannot precisely be differentiated because of their similar radiological features. ^{11}C-methionine positron emission tomography has improved the radiological diagnosis of brain tumors [11]. Among these brain tumors, a finding of low uptake in MET-PET is strongly suggestive of a DNT, and the diagnosis becomes more reliable if associated with corresponding morphology on CT and/or MRI [12,13]. The hypo-uptake in FDG-PET is another characteristic of DNT, which suggests not only the hypometabolism of the tumor but also a lack of functional activity as the normal brain within the lesion. It is this lack of functional activity which permits the complete excision of the tumor without a subsequent postoperative neurological deficit.

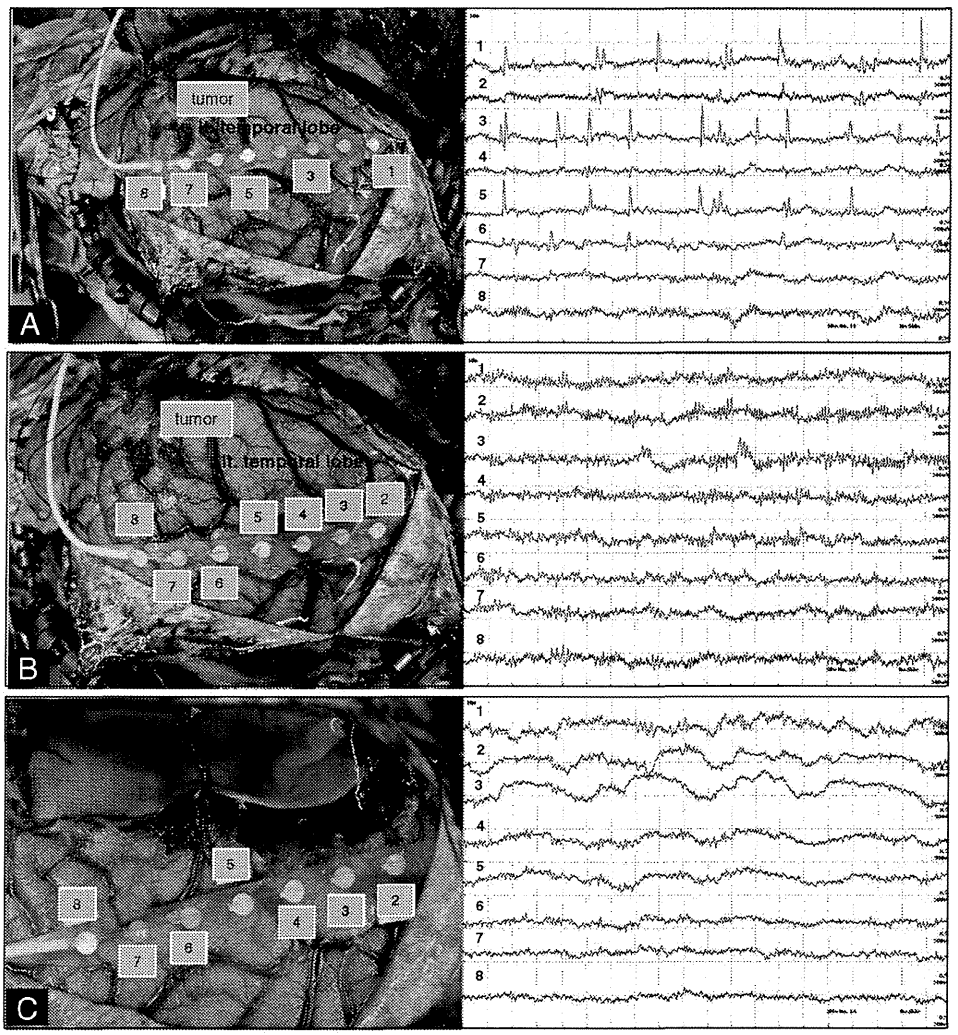

Fig. 7. Case 3. Intraoperative ECoG before lesion resection showing interictal spikes and the representative ECoGs from two different sites (A and B). Epileptiform discharges which emerged on ECoG before lesion resection disappeared after lesion resection on the representative ECoG (C).

Intraoperative ECoG is an essential tool for DNT surgery and is utilized in most surgical procedures for epilepsy [3,4,14–17]. Localization of the EZ associated with a DNT is still controversial, and results are variable. Recently, Chassoux et al. [18] have proposed that three distinct histologic subtypes of DNT are distinguishable based on MRI features. Using MRI, DNTs are classified as type 1 which is cystic/polycystic-like, well-delineated, and strongly hypointense in T1WI; type 2 which is nodular-like and heterogeneous; and type 3 which is dysplastic-like, iso/hypointense in T1WI, with poor delineation and gray–white matter blurring. Resection of type 1 tumors, in which the tumor and the EZ are colocalized, will generally definitively treat the epilepsy. Types 2 and 3, however, require a more extensive resection that includes both the tumor and the perilesional cortex. For example, for type 3 tumors in the temporal lobe, an anterior temporal lobectomy must be considered. Case 2 is a type 1 example and Cases 1 and 3 are type 3 examples. Such a detailed imaging study is informative for preoperative surgical planning for seizure control; however, this is not always helpful to address in delineating the EZ precisely in individual cases. To achieve the objective of seizure control, intraoperative ECoG monitoring is still needed to determine the extent of resection of the lesion including the EZ, although the spike-chasing using ECoG is partly debatable and controversial.

For some DNT, preoperative CT, MRI, interictal EEG, PET studies, and intraoperative ECoG are usually sufficient to achieve seizure control with surgery; however, for others, these are not sufficient. In Case 1, the preoperative interictal EEG did not show any significant epileptogenic activity. Dysembryoplastic neuroepithelial tumor in the temporal lobe, like other epileptic lesions in deep brain structures, often presents with no significant epileptogenic activity in preoperative EEG. In these cases, preoperative chronic subdural electrode recording (CSDER) is strongly recommended to confirm whether the tumor truly has epileptogenicity and to evaluate the extent of the epileptogenic lesion [3,19]. Magnetoencephalography is a sophisticated medical device which can detect subtle brain activity and the epileptogenicity of lesions. Its clinical role for detecting epileptogenicity preoperatively may replace that of CSDER in those cases with visible lesions on neuroimaging because MEG, unlike CSDER, is noninvasive [20–23]. In Case 1, MEG was used instead of CSDER.

The DNT in Case 2 was adjacent to the motor cortex and the language pathway. Epileptogenicity was detectable in the tumor by preoperative EEG. Complex partial seizures observed in this case were likely attributable to tumor extension to the left cingulate gyrus. In this case, treatment planning focused on avoiding damage to the motor cortex and the

language pathway while aiming for total resection of the tumor with the EZ. In such a case, the combination of fiber tractography, neuronavigation system, and SEP is a valuable adjunct to ECoG and imaging studies [24–29]. Preoperative fiber tractography that revealed the topographical relationship between the left pyramidal tract and the tumor and also between the left arcuate fasciculus and the tumor was informative for safe tumor resection. The neuronavigation system and intraoperative SEP aided in the identification of the left central sulcus during the surgery. These interventions were indispensable for preventing surgical complications.

Case 3 had a recurrent large DNT adjacent to the left visual tract, in which epileptogenicity was detectable near the tumor by preoperative EEG. The patient had already had a right upper quadrant hemianopsia from the previous surgery. Another clinicopathological concern in this case was the possibility of malignant transformation of the tumor in terms of its rapid regrowth. Dysembryoplastic neuroepithelial tumor is considered benign and tends to not recur even after a partial resection [1,2]. There are, however, some reported cases of malignant transformation and tumor regrowth [30–33]. To achieve clinical benefit in this patient, the goal of surgery was complete excision of the tumor including malignant parts and EZ without worsening the neurological deficit. Total tumor resection would prevent further regrowth and enable the complete histopathological evaluation of the tumor in addition to seizure control. Tumor resection was successfully performed using the neuronavigation-guided fence-post tube technique in this case. The neuronavigation-guided fence-post technique is superior to ordinary image-guided neuronavigation for larger tumors because intraoperative structural distortion of the brain due to brain shift is more likely during resection of larger tumors [34,35]. Preoperative fiber tractogram, revealing the topographical relationship between the left visual tract and the tumor, was informative for placing fence-posts to define the excision margins. No histological evidence of malignant foci was found in the resected lesion including the tumor. Recently, another case of progressive DNT on MRI in a pediatric patient, in which the tumor showed no histological evidence of malignancy, was reported by Preuss et al. [36]. In such cases, tumor growth is attributed to an increase in the mucinous substance in the myxoid matrix. A further careful follow-up is needed for checking tumor and seizure recurrences in Case 3 because of the short period of follow-up after the second surgery.

4. Conclusions

Although DNT frequently results in epilepsy that is unresponsive to medical therapy, DNT-associated epilepsy is highly curable with surgery. Dysembryoplastic neuroepithelial tumor may arise in any supratentorial or intracortical location within or near critical areas of the brain. Resection, therefore, must be carefully planned both pre- and intraoperatively and requires meticulous technique. Goals of therapy include not only completely resecting the tumor to avoid recurrence or progression but also excising the entire associated EZ. We have shown that when imaging and functional studies are utilized concurrently with advanced neurosurgical technologies for operative planning, excellent surgical outcomes result.

Conflict of interest

None of the authors has any conflict of interest to disclosure.

References

[1] Daumas-Duport C, Scheithauer BW, Chodkiewicz JP, Laws Jr ER, Vedrenne C. Dysembryoplastic neuroepithelial tumor: a surgically curable tumor of young patients with intractable partial seizures. Report of thirty-nine cases. Neurosurgery 1988;23:545–56.

[2] Daumas-Duport C, Pietsch T, Hawkins C, Shankar SK. Dysembryoplastic neuroepithelial tumour. In: Louis DN, Ohgaki H, Wiestler OD, Cavenee WK, editors. WHO classification of tumours of the central nervous system. , World Health Organization classification of tumours, 4th ed.Lyon: International Agency for Research on Cancer; 2007. p. 99–102.

[3] Sandberg DI, Ragheb J, Dunoyer C, Bhatia S, Olavarria G, Morrison G. Surgical outcomes and seizure control rates after resection of dysembryoplastic neuroepithelial tumors. Neurosurg Focus 2005;18(6a):E5.

[4] Chan CH, Bittar RG, Davis G, Kalnins RM, Fabinyi GCA. Long-term seizure outcome following surgery for dysembryoplastic neuroepithelial tumor. J Neurosurg 2006;104:62–9.

[5] Minkin K, Klein O, Mancini J, Lena G. Surgical strategies and seizure control in pediatric patients with dysembryoplastic neuroepithelial tumors: a single-institution experience. J Neurosurg Pediatr 2008;1:206–10.

[6] Bilginer B, yalnizoglu D, Soylemezoglu F, Turanli G, Cila A, Topçu M, et al. Surgery for epilepsy in children with dysembryoplastic neuroepithelial tumor: clinical spectrum, seizure outcome, neuroradiology, and pathology. Childs Nerv Syst 2009;25:485–91.

[7] Spalice A, Ruggieri M, Grosso S, Verrotti A, Polizzi A, Margo G, et al. Dysembryoplastic neuroepithelial tumors: a prospective clinicopathologic and outcome study of 13 children. Pediatr Neurol 2010;43:395–402.

[8] Chang EF, Christie C, Sullivan JE, Garcia PA, Tihan T, Gupta N, et al. Seizure control outcomes after resection of dysembryoplastic neuroepithelial tumor in 50 patients. J Neurosurg Pediatr 2010;5:123–30.

[9] Engel Jr J, Van Ness PC, Rasmusen TB, Ojemann LM. Outcome with respect to epileptic seizures. In: Engel Jr J, editor. Surgical treatment of the epilepsies. 2nd ed. New York: Raven Press; 1993. p. 609–21.

[10] O'Brien DF, Farrell M, Delanty N, Traunecker H, Perrin R, Smyth MD, et al. The Children's Cancer and Leukaemia Group guidelines for the diagnosis and management of dysembryoplastic neuroepithelial tumors. Br J Neurosurg 2007;21:539–49.

[11] Kato T, Shinoda J, Nakayama N, Miwa K, Okumura A, Yano H, et al. Metabolic assessment of gliomas using carbon-11 methionine, fluorine-18 fluorodeoxyglucose, and carbon-11 choline positron-emission tomography. AJNR Am J Neuroradiol 2008;29:1176–82.

[12] Maehara T, Nariai T, Arai N, Kawai K, Shimizu H, Ishii K, et al. Usefulness of [^{11}C] methionine PET in the diagnosis of dysembryoplastic neuroepithelial tumor with temporal lobe epilepsy. Epilepsia 2004;45:41–5.

[13] Rosenberg DS, Demarquay G, Jouvet A, Le Bars D, Streichenberger N, Sindou M, et al. [^{11}C]-methionine PET: dysembryoplastic neuroepithelial tumours compared with other epileptogenic brain neoplasms. J Neurol Neurosurg Psychiatry 2005;76:1686–92.

[14] Kameyama S, Fukuda M, Tomikawa M, Morota N, Oishi M, Wachi M, et al. Surgical strategy and outcomes for epileptic patients with focal cortical dysplasia or dysembryoplastic neuroepithelial tumor. Epilepsia 2001;42(Suppl. 6):37–41.

[15] Nolan MA, Sakuta R, Chuang N, Otsubo H, Rutka JT, Snead III OC, et al. Dysembryoplastic neuroepithelial tumors in childhood. Long-term outcome and prognostic features. Neurology 2004;62:2270–6.

[16] Takahashi A, Hong SC, Seo DW, Hong SB, Lee M, Suh YL. Frequent association of cortical dysplasia in dysembryoplastic neuroepithelial tumor treated by epilepsy surgery. Surg Neurol 2005;64:419–27.

[17] Lee J, Lee BL, Joo EY, Seo DW, Hong SB, Hong SC, et al. Dysembryoplastic neuroepithelial tumors in pediatric patients. Brain Dev 2009;31:671–81.

[18] Chassoux F, Rodrigo S, Mellerio C, Landré E, Miquel C, Turak B, et al. Dysembryoplastic neuroepithelial tumors: an MRI-based scheme for epilepsy surgery. Neurology 2012;79:1699–707.

[19] Seo DW, Hong SB. Epileptogenic foci on subdural recording in intractable epilepsy patients with temporal dysembryoplastic neuroepithelial tumor. J Korean Med Sci 2003;18:559–65.

[20] Medvedovsky M, Taulu S, Gaily E, Metsähonkala EL, Mäkelä JPm Ekstein D, Kipervasser S, et al. Sensitivity and specificity of seizure-onset zone estimation by ictal magnetoencephalography. Epilepsia 2012;53:1649–57.

[21] Kim H, Lim BC, Jeong W, Kim JS, Chae JH, Kim KJ, et al. Magnetoencephalography in pediatric lesional epilepsy surgery. J Korean Med 2012;27:668–73.

[22] Fujiwara H, Greiner HM, Hemasilpin N, Lee KH, Holland-Bouley K, Arthur T, et al. Ictal MEG onset source localization compared to intracranial EEG and outcome: improved epilepsy presurgical evaluation in pediatrics. Epilepsy Res 2012;99:214–24.

[23] Kakisaka Y, Wang ZI, Mosher JC, Nair DR, Alexopoulos AV, Burgess RC. Magnetoencephalography's higher sensitivity to epileptic spikes may elucidate the profile of electroencephalographically negative epileptic seizures. Epilepsy Behav 2012;23:171–3.

[24] Castellano A, Bello L, Michelozzi C, Gallucci M, Fava E, Iadanza A, et al. Role of diffusion tensor magnetic resonance tractography in predicting the extent of resection in glioma surgery. Neuro Oncol 2012;14:192–202.

[25] Fernandez-Miranda JC, Pathak S, Engh J, Jarbo K, Verstynen T, Yeh FC, et al. High-definition fiber tractography of the human brain: neuroanatomical validation and neurosurgical applications. Neurosurgery 2012;71:430–53.

[26] Jung TY, Jung S, Kim IY, Park SJ, Kang SS, Kim SH, et al. Application of neuronavigation system to brain tumor surgery with clinical experience of 420 cases. Minim Invasive Neurosurg 2006;49:210–5.

[27] Tanaka Y, Nariai T, Momose T, Aoyagi M, Maehara T, Tomori T, et al. Glioma surgery using a multimodal navigation system with integrated metabolic images. J Neurosurg 2009;110:163–72.

[28] Suzuki A, Yasui N. Intraoperative localization of the central sulcus by cortical somatosensory evoked potentials in brain tumor. Case report. J Neurosurg 1992;76:867–70.

[29] Hayashi Y, Nakada M, Kinoshita M, Hamada JI. Functional reorganization in the patient with progressing glioma of pure primary motor cortex: a case report with special reference to the topographic central sulcus definition by SEP. World Neurosurg 2013 [in press].

[30] Hammond RR, Duggal N, Woulfe JM, Girvin JP. Malignant transformation of a dysembryoplastic neuroepithelial tumor: case report. J Neurosurg 2000;92:722–5.

[31] Rushing EJ, Thompson LD, Mena H. Malignant transformation of a dysembryoplastic neuroepithelial tumor after radiation and chemotherapy. Ann Diagn Pathol 2003;7:240–4.
[32] Sampetrean O, Maehara T, Arai N, Nemoto T. Rapidly growing dysembryoplastic neuroepithelial tumor: case report. Neurosurgery 2006;59:E1337–8.
[33] Thom M, Toma A, An S, Martinian L, Hadjivassiliou G, Ratilal B, et al. One hundred and one dysembryoplastic neuroepithelial tumors: an adult epilepsy series with immunohistochemical, molecular genetic, and clinical correlations and a review of the literature. J Neuropathol Exp Neurol 2011;70:859–78.
[34] Yoshikawa K, Kajiwara K, Morioka J, Fujii M, Tanaka N, Fujisawa H, et al. Improvement of functional outcome after radical surgery in glioblastoma patients: the efficacy of a navigation-guided fence-post procedure and neurophysiological monitoring. J Neurooncol 2006;78:91–7.
[35] Kajiwara K, Yoshikawa K, Ideguchi M, Nomura S, Fujisawa H, Akimura T, et al. Navigation-guided fence-post tube technique for resection of a brain tumor: technical note. Minim Invasive Neurosurg 2010;53:86–90.
[36] Preuss M, Nestler U, Zühlke CJ, Kuchelmeister K, Neubauer BA, Jödicke A. Progressive biological behavior of a dysembryoplastic neuroepithelial tumor. Pediatr Neurosurg 2010;46:294–8.